

# Understanding the role of temperature in free shear flows via modification of the dynamics of the large scales

By D. J. Bodony†

High-speed mixing layers are known to become quieter when the high-speed stream is heated at constant velocity. The cause of the noise reduction is not known but it is hypothesized that it can be partially explained through modification of the mixing layer's large scale dynamics. It is found through simulations of the linearized dynamics that the large-scale entropy fluctuations play an increasing role with increased temperature, as expected, but also that these fluctuations are partially responsible for reducing the radiated sound. Preliminary results from a multiscale linear theory are developed toward explaining this observation and suggest that the entropy fluctuations are less efficient sound radiators.

---

## 1. Introduction

High-speed turbulent shear layers are an important technological flow with a simple geometric configuration that is ideal for studying inhomogeneous turbulence. Existing work has predominantly focused on the turbulent velocity field, such as its dependence on compressibility effects, because of limitations in experimental measurements of the thermodynamic properties at high speeds and the simplification of assuming local dynamics are isentropic. Non-isothermal mixing layers behave differently from their isothermal counterparts because of changes in the coupling between the thermodynamic fluctuations with the velocity fluctuations which alter turbulent transport and space-time correlations.

Low-speed mixing layers have been studied extensively and much is known about their mean and turbulent velocity fields, as summarized in the reviews of Ho & Huerre (1984) and Dimotakis (1991). The initial growth of the mixing layer is very sensitive to the state of the boundary layer and whether any external forcing or acoustic reflection is present (Bell & Mehta 1990). Asymptotically far away from the splitter plate their width grows linearly with downstream distance in the absence of an externally imposed pressure gradient. Hot-wire measurements of constant property mixing layers by Liepmann & Laufer (1947) and Wignanski & Fiedler (1970) have shown that a simple eddy viscosity assumption can predict reasonably well the mean velocity  $U$  and dominant Reynolds stress  $\langle u'v' \rangle$ , where  $u'$  and  $v'$  are the fluctuating streamwise and transverse velocities, respectively. In addition such measurements have demonstrated the importance of the flow inhomogeneity on intermittency, integral lengthscale variation across the mixing layer, and a frequency-dependent convection velocity.

Instantaneous visualization of low-speed, high-Reynolds-number mixing layers identified the presence of large scale turbulent structures whose growth, and thus that of the time-averaged mixing layer, was a function of the density ratio  $\rho_2/\rho_1$  across the mixing layer (Brown & Roshko 1974). They concluded that compressibility effects were

† Department of Aerospace Engineering, University of Illinois at Urbana-Champaign

more effective at altering the mixing layer growth rate and, subsequently, a large number of investigations were conducted to better understand this (Samimy & Elliott 1990; Goebel *et al.* 1990; Goebel & Dutton 1991; Sandham & Reynolds 1991; Samimy *et al.* 1992; Clemens & Mungal 1995; Vreman *et al.* 1996; Simone *et al.* 1997; Slessor *et al.* 2000; Pantano & Sarkar 2002; Rossmann *et al.* 2002; Kourta & Sauvage 2002; Olsen & Dutton 2003). These studies suggested that the mixing layer growth rate,  $d\delta/dx$ , was a function of a convective Mach number,  $M_c$ , which was loosely linked to the convection velocity of the large structures of the mixing layer. Various definitions for  $M_c$  exist; one of the most commonly used is that of Papamoschou & Roshko (1988) and is  $M_c = (U_1 - U_2)/(a_1 + a_2)$  where  $a_1, a_2$  are the speeds of sound on either side of the mixing layer. However Dimotakis (1991) emphasized that this definition combines the effects of velocity and density ratio and later (Slessor *et al.* 2000) proposed an alternative parameter  $\Pi_c = \max_i(\sqrt{\gamma_i - 1}/a_i)(U_1 - U_2)$  where  $\gamma_i$  is the ratio of specific heats in the  $i$ th stream.

By focusing on the parameter  $M_c$ , the separate effects of velocity ratio and density ratio across high-speed compressible mixing layers have not been examined in great detail, except for the effect of the latter on mixing layer growth (Brown & Roshko 1974; Pantano & Sarkar 2002). Experimentally, it is challenging to measure thermodynamic fields without intrusive diagnostics at the same level of spatiotemporal resolution as provided by particle image velocimetry. Recent enhancements to the measurement capabilities are changing this, however (Mielke *et al.* 2009). In low-speed flows wire-based techniques are available for simultaneous temperature-velocity measurement and Antonia and co-workers have examined in some detail their relationship in mixing layers and in jets (Antonia & Van Atta 1975; Antonia *et al.* 1975; Rajagopalan & Antonia 1981). Others, such as Tong & Warhaft (1995), have used temperature fluctuations in a low-speed flow as a passive scalar proxy for studying turbulent dispersion.

Very little is known about the instantaneous or two-point space-time correlations of velocity with the thermodynamic field in any high-speed turbulent flow, except for a few singular computational efforts (Fortuné *et al.* 2004; Golanski *et al.* 2005; Bodony & Lele 2005, 2008) and recent causality experiments related to jet noise (Panda & Seasholtz 2002; Panda 2007). The successful modeling of noise sources in compressible turbulent flows depends crucially on the space-time correlations of the fluctuations involved and it was recently identified that the velocity-temperature correlation is the largest contributor to noise prediction uncertainty (Bridges *et al.* 2008). It is a commonly held assumption that the  $\langle u'T' \rangle$  space-time correlation is the same as  $\langle u'u' \rangle$ , within a proportionality constant, but there is no simulation or experimental justification for this (Lilley 1996). As a result, current noise prediction methodologies, aside from direct numerical or large-eddy simulation, are unable to predict the trends in jet noise with heating without calibration; nor do we understand the observation that heating a high-speed jet reduces its radiated noise (Tanna 1977; Bodony & Lele 2008).

To this end we examine carefully the dynamical role played by the entropy field through numerical simulations and a multi-scale linear theory. The geometric simplicity of the mixing layer is exploited to simplify the analysis and as a surrogate for future work with axisymmetric shear layers and turbulent jets.

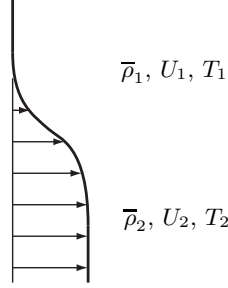


FIGURE 1. Schematic of mixing layer.

## 2. Linearized Euler calculations

We study first the development of disturbances on a spatially developing compressible mixing layer (see Fig. 1) at fixed velocity ratio  $U_1 = 0, U_2 = 1.12a_\infty$  but at varying total temperature ratios  $\text{TR} = T_{t2}/T_{t1} = \{1.00, 1.25, 1.50, 2.00, 2.50, 3.00\}$ . These conditions span those typically found in cold, isothermal, and heated jets in the laboratory. The Mach number of lower, high-speed stream drops from 1.3 to 0.7 as the temperature is raised. To permit comparison with the linear theory presented in the next section, we assume the disturbances are of sufficiently low amplitude but allow them to grow on a turbulent mixing layer. The perturbations to the density, momentum, and total energy,  $\{\rho', (\rho u_i)', (\rho E)'\}$ , are governed by

$$\frac{\partial}{\partial t} \left( \frac{\rho'}{J} \right) + \frac{\partial}{\partial \xi_j} \left( \rho' \hat{U}_j + \bar{\rho} u'_k \hat{\xi}_{j,k} \right) = 0, \quad (2.1)$$

$$\frac{\partial}{\partial t} \left( \frac{(\rho u_i)'}{J} \right) + \frac{\partial}{\partial \xi_j} \left( (\rho u_i)' \hat{U}_j + \bar{\rho} \bar{u}_i u'_k \hat{\xi}_{j,k} + p' \hat{\xi}_{j,i} \right) = 0, \quad (2.2)$$

$$\frac{\partial}{\partial t} \left( \frac{(\rho E)'}{J} \right) + \frac{\partial}{\partial \xi_j} \left( [(\rho E)' + p'] \hat{U}_j + [(\bar{\rho} \bar{E} + \bar{p}) \hat{\xi}_{j,k} u'_k] - p' \hat{\xi}_{j,t} \right) = 0, \quad (2.3)$$

where  $\hat{U}_i = \bar{u}_j \hat{\xi}_{i,j}$  is the mean contravariant velocity and  $\hat{\xi}_{i,j} = J^{-1} \partial \xi_i / \partial x_j$  is the Jacobian-weighted metric. These equations are valid for a calorically perfect gas with equation of state

$$p' = (\gamma - 1) \left\{ (\rho E)' - \frac{1}{2} \bar{\rho} \bar{u}_i u'_i - \frac{1}{2} (\rho u_i)' \bar{u}_i \right\} \quad (2.4)$$

in generalized curvilinear coordinates. The entropy fluctuations  $s'$  about the local mean  $\bar{s}(x, y)$  are given by

$$\frac{s'}{C_v} = \frac{p'}{\bar{p}} - \frac{\gamma p'}{\bar{\rho}}, \quad (2.5)$$

where  $C_v$  is the specific heat at constant volume. Equations (2.1)–(2.5) are dimensional; their non-dimensional forms follow by using the reference quantities from the slow side of the mixing layer:  $\rho_1, c_1 = \sqrt{\gamma R T_1}, (\gamma - 1) T_1, \rho_1 c_1^2, C_v,$  and  $\delta_{\omega,0}$  for the density, velocity, temperature, pressure, entropy, and initial vorticity thickness of the mixing layer, respectively.

The mean flow follows from the observation that most high-Reynolds-number mixing layers are turbulent with a growth rate  $d\delta/dx$  that is a function of the convective Mach number  $M_c = U_2/(a_1 + a_2)$  which is related to the acoustic Mach number  $M_a = U_2/a_1$  and the static temperature ratio  $T_2/T_1$ . We thus propose the following mean flow based

on empirical data:

$$\bar{u}(x, y) = \frac{M_a}{2} \left( 1 - \operatorname{erf} \left\{ \frac{y}{\delta(x)} \right\} \right), \quad (2.6)$$

$$\bar{v}(x, y) = 0, \quad (2.7)$$

$$\bar{p}(x, y) = p_\infty, \quad (2.8)$$

$$\bar{\rho}(x, y) = \frac{\gamma p_\infty}{(\gamma - 1) \bar{T}(x, y)}, \quad (2.9)$$

where

$$\delta(x) = \begin{cases} 1/\sqrt{\pi}, & x \leq x_a \\ 1/\sqrt{\pi} + 2S(1 - \operatorname{erf}(0.6M_c x)), & x \geq x_c, \end{cases} \quad (2.10)$$

where  $S = 0.10$  is an estimate of incompressible turbulent mixing layer growth (Pope 2000) and  $1 - \operatorname{erf}(0.6M_c x)$  is the compressibility correction to it. Observe that for  $x \leq x_a$  the mixing layer is parallel and for  $x \geq x_c$  the mixing layer grows linearly; for  $x_a \leq x \leq x_c$  a circular fillet blends the two growth rates. Finally, the mean density follows from the assumption of constant mean pressure and the Crocco-Busemann relation,

$$\bar{T}(x, y) = -\frac{1}{2}\bar{u}^2 + C_1\bar{u} + C_2 \quad (2.11)$$

where  $C_1 = (1 - T_2/T_1)/(\gamma - 1) + M_a/2$  and  $C_2 = (T_2/T_1)/(\gamma - 1) + M_a^2/2 - M_a C_1$ .

### 2.1. Incident spatial instability waves

To perturb the shear layer, linear waves from a spatial instability analysis are added through the inflow boundary condition and through an upstream sponge region (Bodony 2006). The sponge, which adds a term  $-\sigma(x)(\vec{q} - \vec{q}_t)$  to the right-hand-side of the governing equations, drives the current solution  $\vec{q} = \{\rho', (\rho\vec{u})', (\rho E)'\}$  to the target solution  $\vec{q}_t$ , the latter of which comes from instability theory. By assuming the ansatz  $\vec{q}_t = \vec{q}(y) \exp\{i(\alpha x - \omega t)\}$ , with  $\omega > 0$ , a single second order differential equation for the vertical velocity  $\hat{v}(y)$  eigenfunction results with  $\alpha$  the complex eigenvalue. The real and imaginary parts of  $\alpha$  are shown in Fig. 2 as a function of the non-dimensional frequency  $\operatorname{St} = (\omega/2\pi)M_a^{-1}(D_j/\theta_0)(\theta_0/\delta_{\omega,0})$  where, based on a  $D_j = 1$  inch diameter nozzle, at laboratory conditions  $D_j/\theta_0 = 254$ , and  $\theta_0/\delta_{\omega,0} = 0.23$ , for momentum thickness of  $\theta_0 = 0.1$  mm.

### 2.2. Numerical method

Equations (2.1)–(2.5), in non-dimensional form, were solved using a globally third-order accurate summation-by-parts approximation with an explicit norm (Strand 1994); the scheme is second order on boundaries and fourth order in the interior. The boundary conditions utilized the simultaneous-approximation-term approach (Svärd *et al.* 2007) modified for the current linearized equations. The time advancement used a traditional fourth-order Runge-Kutta method with a fixed timestep corresponding to a CFL of approximately 0.4. This approach has been shown to be stable and accurate for a variety of problems in aeroacoustics (Bodony 2010).

### 2.3. Single frequency results

Results from the linearized simulations are presented here for a single frequency case of  $\omega = 0.1a_\infty/\delta_{\omega,0}$ ; multi-frequency results will be presented elsewhere. After the instability

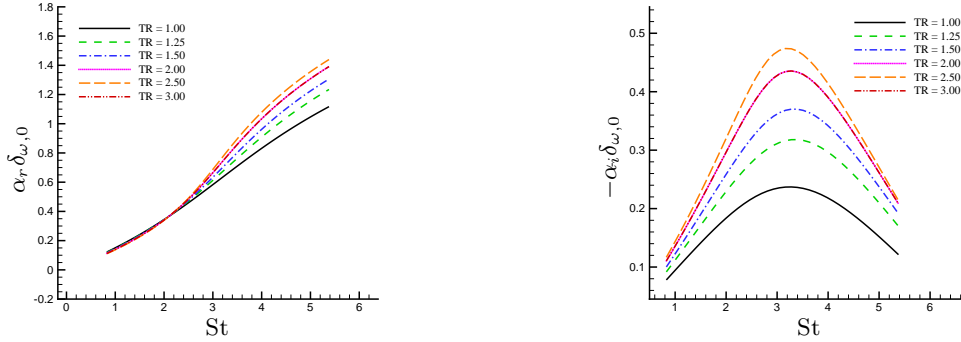


FIGURE 2. Linear instability wavenumber  $\alpha_r$  (left) and growth rate  $-\alpha_i$  (right) for a heating planar mixing layer with constant velocity  $U_1 = 0$ ,  $U_2 = 1.12a_\infty$ , and varying total temperature ratio  $TR = T_{t2}/T_{t1}$ .

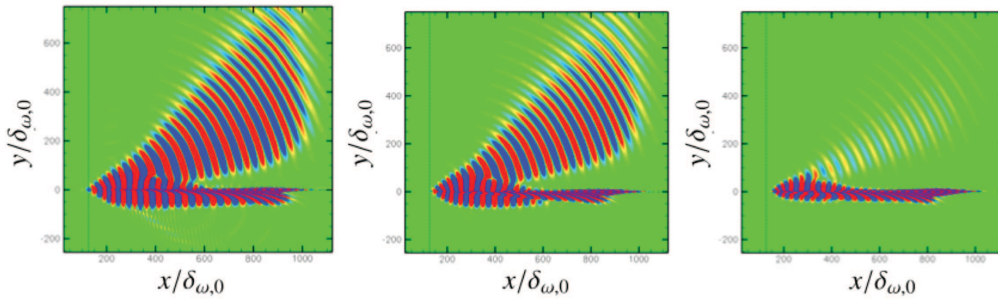


FIGURE 3. Instantaneous density perturbation  $\rho'$  for the cold (TR = 1.0, left), isothermal (TR = 1.25, middle), and heated (TR = 2.00, right) mixing layers. Vertical dashed line corresponds to end of sponge region.

waves are introduced, a transient period follows after which a steady, sinusoidal temporal response of all points in space is observed. At the steady state root-mean-square velocity, pressure, and entropy fluctuations are recorded. The varying growth rates of the instability waves with temperature imply that the peak fluctuation levels will be different for a fixed given initial disturbance amplitude. Thus, to put the simulations on an equal footing, the linear results are scaled such that the peak level of  $u'$  root-mean-square along  $y = 0$  is unity. Justification for this scaling comes from the experimental observation that in heated jets the mixing layer fluctuation levels are approximately constant for fixed velocity (Bridges & Wernet 2003). The scaling factors, relative to the cold mixing layer, where  $A \in \{1.00, 1.99, 4.41, 22.10, 77.47, 189.53\}$ , in a trend consistent with the increase in  $-\alpha_i$  with increasing TR. All fields are scaled accordingly.

A visualization of the scaled  $\rho'$  and the mean streamwise velocity is given in Fig. 3 for a mixing layer at three different temperature ratios corresponding to cold, isothermal, and heated. It is observed that above the mixing layer the density field diminishes in amplitude with increasing temperature, consistent with experimental data on high-speed jets.

A more quantitative view is given in Fig. 4, which shows the scaled streamwise velocity, pressure, and entropy root-mean-square values, as functions of the temperature ratio, along  $y = 0$ . Observe that in Fig. 4a the peak velocity for each curve is one, though

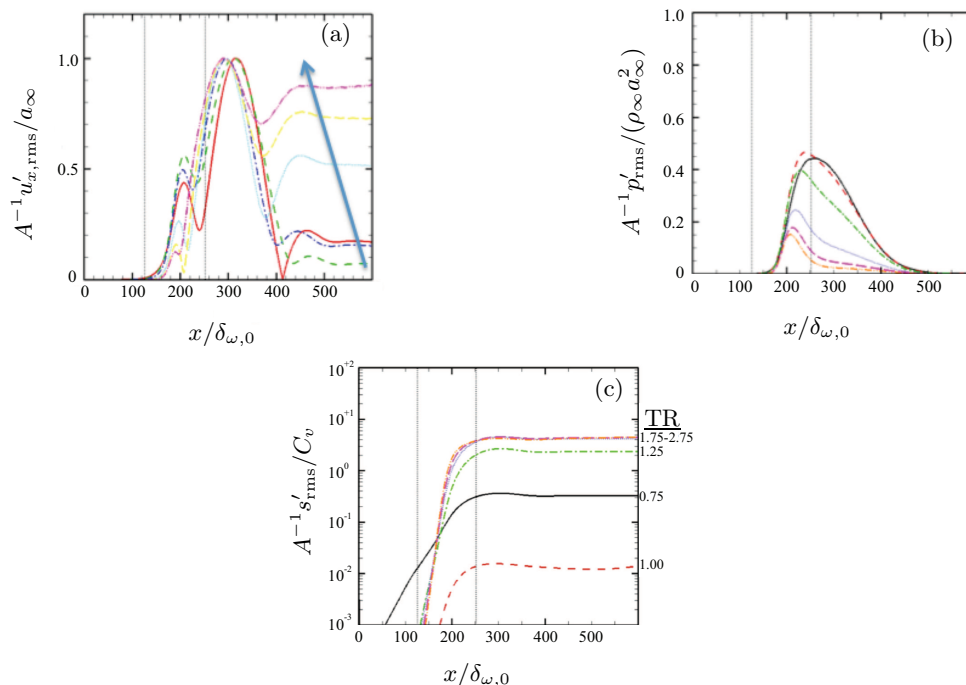


FIGURE 4. Normalized fluctuations from linear analysis of a  $\Delta U = 1.12a_{\infty}$  shear layer. Arrow shows increasing ratio of  $T_{i2}/T_{i1}$ . (a): scaled  $u'_x$ . (b): scaled  $p'$ . (c): scaled  $s'$ . The vertical lines correspond to  $x_a$  and  $x_c$ , respectively.

the peak location moves upstream with heating. After the peak value of  $u'_x$  there is a local minimum followed by a secondary rise whose value at large  $x/\delta_{\omega,0}$  approaches a constant that depends on the temperature ratio. The pressure fluctuations, in contrast, exhibit a single peak and then rapidly decay downstream. The peak pressure fluctuation diminishes with increased heating. Finally, the entropy fluctuations show an exponential rise followed by a plateau at large downstream locations without a distinct maximum. The entropy plateau amplitude is minimum for the isothermal mixing layer and increases with increasing temperature ratio. It appears from the data in Fig. 4 that the velocity and entropy fields become tightly coupled downstream in the mixing layer whereas the pressure field is initially coupled to the velocity but then is not continuously generated, resulting in a single-peaked profile. This latter observation is also found in the far-field directivity as shown in Fig. 5 where the pressure fluctuations as a function of angle from the downstream mixing layer axis diminish monotonically with increasing temperature.

### 3. Multiscale linear theory

The numerical results in the previous section are consistent with large scale nonlinear simulations and with experiment where heating a high-speed shear flow reduces its radiated sound. To explain the observations we appeal to linear theory and follow the approach of Tam & Morris (1980). Only preliminary results are available at this time, which are as follows. The mean flow used varies slowly in the  $x$ -direction but has rapid variation in the  $y$ -direction, which suggests introducing a slow coordinate  $X = \epsilon x$  where  $\epsilon \ll 1$  is a measure of the growth rate  $d\delta/dx$ . In doing so suppose we expand  $\vec{u}$  as

$[U(y/X), \epsilon V(y/X)]^T$  and propose for the perturbations the ansatz

$$\vec{q}' = \left\{ \sum_{n=0}^{\infty} \epsilon^n \hat{q}_n(y, X) \right\} \exp[i(\theta(X) - \omega t)], \quad (3.1)$$

where  $d\theta/dx = \alpha(X)$  is the local wavenumber and  $\omega$  is the real-valued frequency as before. After substituting Eq. (3.1) into Eqs. (2.1)–(2.3), the order unity equations may be combined into a single second order differential equation for  $\hat{p}_0$ , the pressure disturbance, as

$$\frac{d^2 \hat{p}_0}{dy^2} + \left[ \frac{2\alpha}{\hat{\omega}} \frac{dU}{dy} + \frac{1}{\gamma} \frac{d\bar{s}}{dy} \right] \frac{d\hat{p}_0}{dy} - [\alpha^2 - \hat{\omega}^2 M_a^2 \bar{\rho}] \hat{p}_0 = 0, \quad (3.2)$$

where  $\hat{\omega} = \omega - \alpha U$ . Equation (3.2) depends on both the mean velocity and mean entropy gradients and describes the same dynamics as the linear instability waves from §2.1.

Shown in Fig. 6 are the order unity solutions to Eq. (3.2). As the mixing layer grows the eigenvalue  $\alpha$  of the unstable modes shown in Fig. 2 changes, as seen in Fig. 6(b) and Fig. 6(c). As the mode becomes damped the critical layer  $y^*$ , defined by  $\hat{\omega}(y^*) = \omega - U(y^*) = 0$ , crosses the real axis in the complex  $y$ -plane and one must integrate around it. To do this the method of Boyd (1985) is adopted where Eq. (3.2) is integrated in the complex  $y$ -plane by parameterizing the integration path  $y = \mathcal{Y}(x)$ , with  $x$  real, by the simple mapping

$$y = x + i\Delta \exp \left\{ \frac{-(x - \zeta)^2}{\sigma^2} \right\} \quad (3.3)$$

with  $\Delta = 0.10 + \text{Im}(y^*)$ ,  $\zeta = y - \text{Re}(y^*)$ , and  $\sigma = 0.1$ . The integral  $\int_0^x \alpha(x') dx'$  equals the phase  $\theta(x)$  function required in Eq. (3.1).

When coupled to evanescent boundary conditions at  $|y| \rightarrow \infty$  the solution  $\hat{p}_0$  is not uniformly valid away from the mixing layer as  $x \rightarrow \infty$  and must be coupled to a global solution via the method of matched asymptotics. It can be shown that the far-field acoustic solution, obtained after matching terms at intermediate values of  $y$  above the mixing layer, is of the form

$$p'(r, \theta, t) = \sum_{n=0}^{\infty} \epsilon^n \int_{-\infty}^{\infty} \bar{g}_n(k) \exp[i(-\sqrt{M_a^2 \omega^2 - k^2} \sin \theta + k \cos \theta)r - i\omega t] dk, \quad (3.4)$$

where  $\bar{g}_n(k)$  is the  $x$ -Fourier transform of the amplitude function  $g_n(x)$  of the pressure fluctuations along the centerline, as shown in Fig. 3b. Extracting  $g_n(x)$  from the time-domain data requires an adjoint calculation to ensure orthogonality between  $\hat{p}_0$  and its adjoint, a procedure which is not yet complete.

#### 4. Concluding remarks

Preliminary results from the analysis of a planar, two-dimensional high-speed mixing layer at non-isothermal conditions show consistency with observations from experiments and non-linear large-eddy simulations of high-speed turbulent jets where the radiated sound decreases with increasing temperature ratio. The cause of the reduction is not yet known but is believed to be related to the emergence of significant entropy fluctuations within the mixing layer created by the spatially varying mean velocity and mean entropy gradients. A multiscale linear theory suggests a path for explaining the observations by coupling a multiscale expansion near the mixing layer to a globally valid outer problem through the method of matched asymptotic expansions.

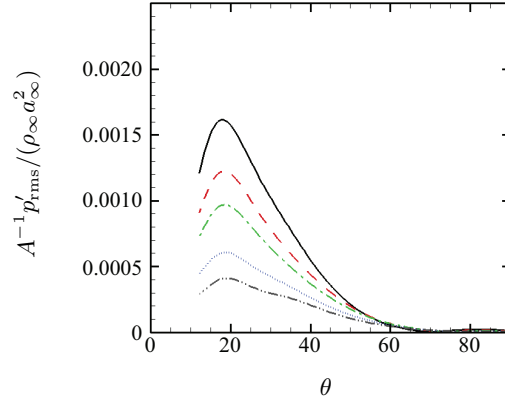


FIGURE 5. Directivity of pressure fluctuations on an arc of radius  $600\delta_{\omega,0}$  from the end of sponge zone.

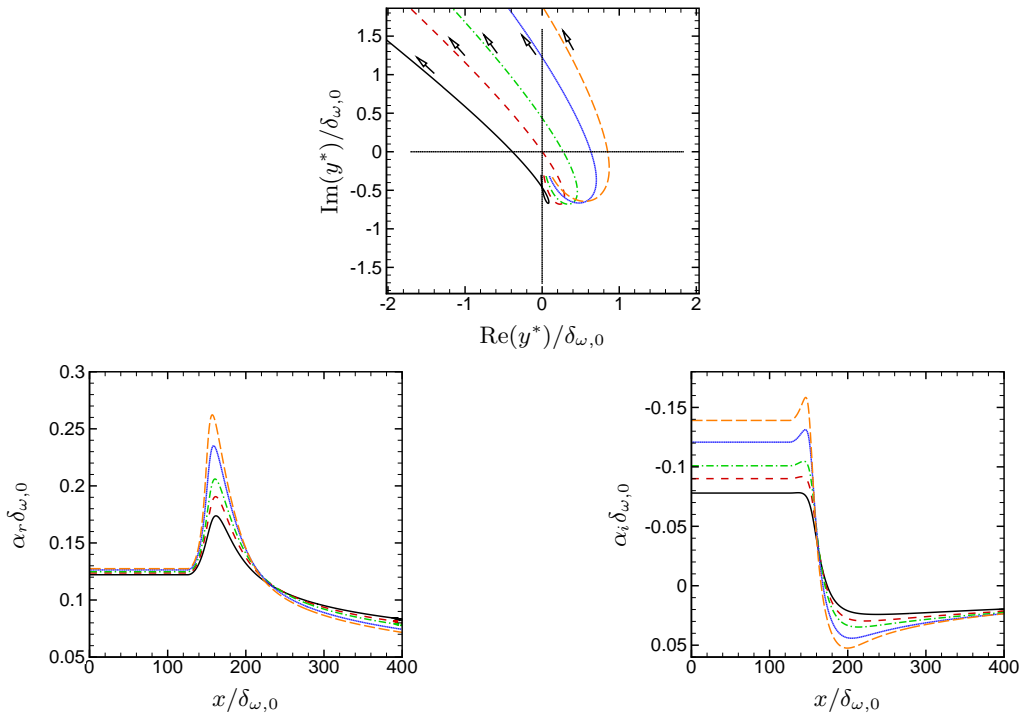


FIGURE 6. Solution of Eq. (3.2) for mixing layer showing critical layer  $y^*$  (top middle), real part of wavenumber  $\alpha_r$  (lower left) and imaginary part  $\alpha_i$  (lower right), as a function of position  $x$ . Legend same as Fig. 2.

### 5. Acknowledgments

This work received financial support from NASA (Supersonic Fixed Wing Program Award Number NNX07AC94A, technical monitors Dr. James Debonis and Dr. James Bridges; and, Subsonic Fixed Wing Program Award Number NNX07AB90A, technical monitor Dr. Lennart S. Hultgren). Comments on a draft of this report by Dr. Joseph Nichols (CTR) are gratefully acknowledged.

## REFERENCES

- ANTONIA, R. A., PRABHU, A. & STEPHENSON, S. E. 1975 Conditionally sampled measurements in a heated turbulent jet. *J. Fluid Mech.* **72** (3), 455–480.
- ANTONIA, R. A. & VAN ATTA, C. W. 1975 On the correlation between temperature and velocity dissipation fields in a heated turbulent jet. *J. Fluid Mech.* **67** (2), 273–288.
- BELL, J. H. & MEHTA, R. D. 1990 Development of a two-stream mixing layer from tripped and untripped boundary layers. *AIAA J.* **28** (12), 2034–2042.
- BODONY, D. J. 2006 Analysis of sponge zones for computational fluid mechanics. *J. Comp. Phys.* **212**, 681–702.
- BODONY, D. J. 2010 Accuracy of the simultaneous-approximation-term boundary condition for time-dependent problems. *J. Sci. Comput.* **43** (1), 118–133.
- BODONY, D. J. & LELE, S. K. 2005 On using large-eddy simulation for the prediction of noise from cold and heated turbulent jets. *Phys. Fluids* **17** (085103).
- BODONY, D. J. & LELE, S. K. 2008 Low frequency sound sources in high-speed turbulent jets. *J. Fluid Mech.* **617**, 231–253.
- BOYD, J. P. 1985 Complex coordinate methods for hydrodynamic instabilities and Sturm-Liouville eigenproblems with an interior singularity. *J. Comput. Phys.* **57**, 454–471.
- BRIDGES, J., KHAVARAN, A. & HUNTER, C. A. 2008 Assessment of current jet noise prediction capabilities. AIAA Paper 2008-2933, Presented at the 14th AIAA/CEAS Aeroacoustics Conference and Exhibit.
- BRIDGES, J. & WERNET, M. P. 2003 Measurements of the aeroacoustic sound source in hot jets. AIAA Paper 2003-3130, Presented at the 9th AIAA/CEAS Aeroacoustics Conference and Exhibit, Hilton Head Island, SC, May 12–14.
- BROWN, G. L. & ROSHKO, A. 1974 On density effects and large structure in turbulent mixing layers. *J. Fluid Mech.* **64**, 775–816.
- CLEMENS, N. T. & MUNGAL, M. G. 1995 Large-scale structure and entrainment in the supersonic mixing layer. *J. Fluid Mech.* **284**, 171–216.
- DIMOTAKIS, P. E. 1991 Turbulent free shear layer mixing and combustion. In *Progress in Aeronautics and Astronautics* (ed. Murthy & Curran), , vol. 137. AIAA.
- FORTUNÉ, V., LAMBALLAIS, É. & GERVAIS, Y. 2004 Noise radiated by a non-isothermal, temporal mixing layer. part i: Direct computation and prediction using compressible dns. *Theor. Comp. Fluid. Dyn.* **18**, 61–81.
- GOEBEL, S. G. & DUTTON, J. C. 1991 Experimental study of compressible turbulent mixing layers. *AIAA J.* **29** (4), 538–546.
- GOEBEL, S. G., DUTTON, J. C., KRIER, H. & RENIE, J. P. 1990 Mean and turbulent velocity measurements of supersonic mixing layers. *Exp. Fluids* **8**, 263–272.
- GOLANSKI, F., FORTUNÉ, V. & LAMBALLAIS, É. 2005 Noise radiated by a non-isothermal, temporal mixing layer. part ii: Prediction using dns in the framework of low mach number approximation. *Theor. Comp. Fluid. Dyn.* **19** (6), 391–416.
- HO, C.-M. & HUERRE, P. 1984 Perturbed free shear layers. *Ann. Rev. Fluid Mech.* **16**, 365–424.
- KOURTA, A. & SAUVAGE, R. 2002 Computation of supersonic mixing layers. *Phys. Fluids* **14** (11), 3790–3797.
- LIEPMANN, H. W. & LAUFER, J. 1947 Investigations of free turbulent mixing. Technical Note TN-1257. NACA.

- LILLEY, G. M. 1996 The radiated noise from isotropic turbulence with applications to the theory of jet noise. *J. Sound Vib.* **190** (3), 463–476.
- MIELKE, A. F., ELAM, K. A. & SUNG, C.-J. 2009 Multiproperty measurements at high sampling rates using rayleigh scattering. *AIAA J.* **47** (4), 850–862.
- OLSEN, M. G. & DUTTON, J. C. 2003 Planar velocity measurements in a weakly compressible mixing layer. *J. Fluid Mech.* **486**, 51–77.
- PANDA, J. 2007 Experimental investigation of turbulent density fluctuations and noise generation from heated jets. *J. Fluid Mech.* **591**, 73–96.
- PANDA, J. & SEASHOLTZ, R. G. 2002 Experimental investigation of density fluctuations in high-speed jets and correlation with generated noise. *J. Fluid Mech.* **450**, 97–130.
- PANTANO, C. & SARKAR, S. 2002 A study of compressibility effects in the high-speed turbulent shear layer using direct simulation. *J. Fluid Mech.* **451**, 329–371.
- PAPAMOSCHOU, D. & ROSHKO, A. 1988 The compressible turbulent shear layer: an experimental study. *J. Fluid Mech.* **197**, 453–477.
- POPE, S. B. 2000 *Turbulent Flows*. Cambridge, U.K.: Cambridge University Press.
- RAJAGOPALAN, S. & ANTONIA, R. A. 1981 Properties of the large structure in a slightly heated turbulent mixing layer of a plane jet. *J. Fluid Mech.* **105**, 261–281.
- ROSSMANN, T., MUNGAL, M. G. & HANSON, R. K. 2002 Evolution and growth of large-scale structures in high compressibility mixing layers. *J. Turbulence* **3** (9), 2–19.
- SAMIMY, M. & ELLIOTT, G. S. 1990 Effect of compressibility on the characteristics of free shear layers. *AIAA J.* **28** (3), 439–445.
- SAMIMY, M., REEDER, M. F. & ELLIOTT, G. S. 1992 Compressibility effects on large structures in free shear flows. *Phys. Fluids A* **4** (6), 1251–1257.
- SANDHAM, N. D. & REYNOLDS, W. C. 1991 Three-dimensional simulations of large eddies in the compressible mixing layer. *J. Fluid Mech.* **224**, 133–158.
- SIMONE, A., COLEMAN, G. N. & CAMBON, C. 1997 The effect of compressibility on turbulent shear flow: a rapid-distortion-theory and direct numerical study. *J. Fluid Mech.* **330**, 307–338.
- SLESSOR, M. D., ZHUANG, M. & DIMOTAKIS, P. E. 2000 Turbulent shear-layer mixing: growth-rate compressibility scaling. *J. Fluid Mech.* **414**, 35–45.
- STRAND, B. 1994 Summation by parts for finite difference approximations for  $d/dx$ . *J. Comput. Phys.* **110**, 47–67.
- SVÄRD, M., CARPENTER, M. H. & NORDSTRÖM, J. 2007 A stable high-order finite difference scheme for the compressible navier-stokes equations, far-field boundary conditions. *J. Comput. Phys.* **225**, 1020–1038.
- TAM, C. K. W. & MORRIS, P. J. 1980 The radiation of sound by the instability waves of a compressible plane turbulent shear layer. *J. Fluid Mech.* **98** (2), 349–381.
- TANNA, H. K. 1977 An experimental study of jet noise part i: Turbulent mixing noise. *J. Sound Vib.* **50** (3), 405–428.
- TONG, C. & WARHAFT, Z. 1995 Passive scalar dispersion and mixing in a turbulent jet. *J. Fluid Mech.* **292**, 1–38.
- VREMAN, A. W., SANDHAM, N. D. & LUO, K. H. 1996 Compressible mixing layer growth rate and turbulence characteristics. *J. Fluid Mech.* **330**, 235–258.
- WYGNANSKI, I. & FIEDLER, H. E. 1970 The two-dimensional mixing region. *J. Fluid Mech.* **41** (2), 327–361.